Geochimica et Cosmochimica Acta, Vol. 69, No. 3, pp. 607–621, 2005

0016-7037/05 $30.00 + .00

doi:10.1016/j.gca.2004.08.006

The dissolution kinetics of a granite and its minerals—Implications for comparison between laboratory and field dissolution rates

JIWCHAR GANOR,[1,*] EMMANUELLE ROUEFF,[1] YIGAL EREL,[2] AND JOEL D. BLUM[3]

[1]Department of Geological and Environmental Sciences, Ben-Gurion University of the Negev, P.O. Box 653, Beer-Sheva 84105, Israel
[2]Institute of Earth Sciences, The Hebrew University of Jerusalem, Jerusalem 91904, Israel
[3]Department of Geological Sciences, University of Michigan, Ann Arbor, MI 48109-1063, USA

(*Received February* 13, 2004; *accepted in revised form August* 12, 2004)

Abstract—The present study compares the dissolution rates of plagioclase, microcline and biotite/chlorite from a bulk granite to the dissolution rates of the same minerals in mineral-rich fractions that were separated from the granite sample. The dissolution rate of plagioclase is enhanced with time as a result of exposure of its surface sites due to the removal of an iron oxide coating. Removal of the iron coating was slower in the experiment with the bulk granite than in the mineral-rich fractions due to a higher Fe concentration from biotite dissolution. As a result, the increase in plagioclase dissolution rate was initially slower in the experiment with the bulk granite. The measured steady state dissolution rates of both plagioclase ($6.2 \pm 1.2 \times 10^{-11}$ mol g^{-1} s^{-1}) and microcline ($1.6 \pm 0.3 \times 10^{-11}$ mol g^{-1} s^{-1}) were the same in experiments conducted with the plagioclase-rich fraction, the alkali feldspar-rich fraction and the bulk granite.

Based on the observed release rates of the major elements, we suggest that the biotite/chlorite-rich fraction dissolved non-congruently under near-equilibrium conditions. In contrast, the biotite and chlorite within the bulk granite sample dissolved congruently under far from equilibrium conditions. These differences result from variations in the degree of saturation of the solutions with respect to both the dissolving biotite/chlorite and to nontronite, which probably was precipitating during dissolution of the biotite and chlorite-rich fraction. Following drying of the bulk granite, the dissolution rate of biotite was significantly enhanced, whereas the dissolution rate of plagioclase decreased.

The presence of coatings, wetting and drying cycles and near equilibrium conditions all significantly affect mineral dissolution rates in the field in comparison to the dissolution rate of fully wetted clean minerals under far from equilibrium laboratory conditions. To bridge the gap between the field and the laboratory mineral dissolution rates, these effects on dissolution rate should be further studied.

1. INTRODUCTION

Weathering rates of silicate minerals observed in the laboratory are in general up to three orders of magnitude higher than those inferred from field studies (Schnoor, 1990; Stumm, 1992; van Grinsven and van Riemsdijk, 1992; Anbeek, 1993; Casey et al., 1993; Velbel, 1993; Blum and Stillings, 1995; White and Brantley, 1995; Drever, 2003; White and Brantley, 2003). The many differences between experimental conditions in the laboratory and natural conditions in the field have been thoroughly discussed in previous studies (e.g., White and Brantley, 2003), and thus will not be repeated here. One of these differences is that most dissolution experiments are conducted using a single mineral, whereas most silicate rocks are composed of several major minerals. To contribute to understanding differences between the field and the laboratory, the present study compares the dissolution rates of plagioclase, microcline, and biotite/chlorite from a bulk sample of the Elat Granite to the dissolution rates of the same minerals in single mineral-rich fractions that were separated from the same granite sample. All the experiments were conducted in the same laboratory, using the same laboratory procedures, and at the same pH and temperature.

Most dissolution experiments use very pure and clean samples, usually from pegmatites, hydrothermal veins, or even synthetic minerals. Rock samples, in contrast, contain in addition to the major minerals, traces of other minerals as well as amorphous phases. These trace minerals may be inclusions inside the major minerals or coatings on the mineral surfaces. For the present study, we chose a hydrothermally altered granite sample. As a result of the hydrothermal activity the major minerals have been partly altered and coated by secondary minerals. Mineral samples that are stained red due to iron oxide coatings are usually regarded as inappropriate for dissolution experiments. However, such coatings, which are a feature of many rock samples, may influence the dissolution rate of the coated minerals. (e.g., Mogollon et al., 1996; Nugent et al., 1998; Hodson, 2003; Metz et al., 2005).

In contrast to many field situations, in which the dissolving minerals are exposed to cycles of wetting and drying, mineral surfaces are constantly in contact with solutions throughout a typical dissolution experiment. In the present study the dissolution experiment with the bulk granite was stopped after 1200 h, the sample was kept dry for 50 d, and then the experiment was resumed. As will be shown below, drying had an important effect on the dissolution rate when the experiment was resumed.

The major element, trace element and isotopic compositions of the output solutions of all the experiments were analyzed. The present paper focuses on the results of the major element analyses. The changes in the trace element and isotopic com-

* Author to whom correspondence should be addressed (ganor@bgumail.bgu.ac.il).

positions during the dissolution of the bulk granite and the mineral-rich fractions are discussed in Erel et al. (2004).

2. MATERIALS AND METHODS

The rock used for the dissolution experiments, the Elat Granite from the Nahal Shlomo pluton (Israel), is a medium- to coarse- grained granite. The mineralogy of the granite was initially characterized using polarized light microscopy. Polished thin sections of the Elat Granite were carbon-coated and constituent minerals were chemically analyzed using a JEOL JXA-8600 electron microprobe. The uncertainties of the measured oxide concentrations were better than ± 5% for concentrations above 40 wt%. The uncertainty increases to ± 15 and 20% for measurements at lower concentrations of 10 wt% and 5 wt%, respectively.

Rock samples were initially crushed in a jaw crusher and then in a disk mill, and the samples were sieved to isolate the 150–250 μm size fraction. Four mineral fractions: plagioclase-rich, alkali feldspar-rich, biotite + chlorite-rich, and quartz-rich were separated by utilizing contrasts in the densities and magnetic properties of the various minerals. After separation, the bulk granite and the mineral-rich fractions were further ground to 75–150 μm diameter grain size. Aliquots from the bulk granite and the plagioclase- and alkali feldspar-rich fractions were digested with concentrated HF and HNO_3 for trace element and isotopic analyses and fused with Li-metaborate and dissolved in dilute HNO_3 for major element analysis. Details of the procedure can be found in Erel et al. (2004).

Dissolution experiments with the bulk granite and with the plagioclase-, the alkali feldspar- and the biotite/chlorite-rich fractions were carried out using flow-through reactors, at flow rate of 0.017 mL min^{-1}, pH 1 and a temperature of 25°C, using ultrapure dilute HNO_3 as the input solution. Approximately 3 g of the 75–150 μm size fraction were introduced into the reactor, and dissolution experiments were run for a few thousand hours. The experiment with the bulk granite was halted after 1220 h, the crushed granite was taken out of the cell, dried at 50°C for ~50 d, and then the experiment was resumed. The mineral-rich fractions were not dried during the course of the experiments. At ~1500 h after the beginning of the experiment with the biotite/chlorite-rich fraction the flow was stopped for 2 d, due to a problem with the inlet tubing, and then resumed. Details of the experimental set-up can be found in Erel et al. (2004).

Al, Si, Mg, Ca, K, Fe, Na, Ti and Mn concentrations in the output solutions were measured by Inductively Coupled Plasma Atomic Emission Spectroscopy (ICP-AES, Perkin-Elmer 3000). The uncertainty in ICP-AES measurements was better than ± 5%. The pH was measured at 25°C on an unstirred aliquot of solution using a WTW combination electrode, with a reported accuracy of ± 0.01 pH units.

3. CALCULATIONS

The release rate (mol s^{-1}) of an element, j, in a well-mixed flow-through experiment is obtained from the expression:

$$Rate_j = \frac{dC_{j,out}}{dt} \cdot V + q\left(C_{j,out} - C_{j,inp}\right) \quad (1)$$

where $C_{j,inp}$ and $C_{j,out}$ are the concentration of component j in the input and the output solutions (mol m^{-3}), t is time (s), V is the volume of the cell (m^3) and q is the fluid volume flux through the system (m^3 s^{-1}). The input solutions in the experiments contained only pure dilute HNO_3 and therefore Eqn. 1 becomes

$$Rate_j = \frac{dC_{j,out}}{dt} \cdot V + q \cdot C_{j,out} \quad (2)$$

The time derivative of the concentration (dC/dt) in Eqn. 2 was approximated by the change in concentration with time ($\Delta C/\Delta t$) at each point of time, i, which was calculated from the slope of the concentration vs. time between the previous point ($i - 1$) and the following point ($i + 1$), i.e.,

$$\frac{dC_{j,out}}{dt} \approx \frac{\Delta C_{j,out}}{\Delta t} = \frac{3 \cdot \left(C_{i-1} \cdot t_{i-1} + C_i \cdot t_i + C_{i+1} \cdot t_{i+1}\right) - \left(C_{i-1} + C_i + C_{i+1}\right) \cdot \left(t_{i-1} + t_i + t_{i+1}\right)}{3 \cdot \left(t_{i-1}^2 + t_i^2 + t_{i+1}^2\right) - \left(t_{i-1} + t_i + t_{i+1}\right)^2} \quad (3)$$

At steady state, the composition of the output solution reaches a constant value [$(dC_{j,out}/dt) = 0$], and therefore the steady state rate ($Rate_{j,ss}$) was calculated by

$$Rate_{j,ss} = q \cdot C_{j,out} \quad (4)$$

Achievement of steady state was defined as a series of samples in which the concentrations of the major elements were constant, where constancy was defined as output concentrations that differed by less than ± 10%. The error in the calculated rates ($\Delta Rate$) is estimated using the Gaussian error propagation method (Barrante, 1974) from the equation

$$\Delta Rate = \left[\sum_i \left(\frac{\partial Rate}{\partial x_i}\right)^2 \left(\Delta x_i^2\right)\right]^{1/2} \quad (5)$$

where Δx_i is the estimated uncertainty in the measurements of the quantity x_i. For most of the experiments, the errors in the calculated elemental release rates usually ranged from 4 to 10%. The exceptions were stages in which the experimental conditions were unstable, usually due to fluctuations in flow rate, where the error may have been significantly larger.

4. RESULTS

4.1. Chemistry of Bulk Granite and the Mineral-Rich Fractions

In the present study we used a granite sample for which there is evidence of alteration by hydrothermal fluids shortly after crystallization of the granite. The feldspars in this sample have been partly replaced by sericite and stained red due to iron oxide coatings; the biotite has been partly transformed to chlorite. Alteration products occur both on the mineral surfaces and within microscopic cracks that cut through the grains. The granite contains two different compositions of plagioclase: a free plagioclase with a composition of oligoclase (Table 1) and plagioclase exsolution lamellae within the perthitic alkali feldspar. The perthitic alkali feldspar has irregular vein patch perthite texture, the constituents of which are composed of an almost pure end member albite and microcline. Due to its complex perthitic texture, it is not possible to determine the relative percentage of the microcline and the albite in the alkali feldspar using the electron microprobe measurements. Biotite occurs in euhedral flakes and elongated aggregates. Due to the strong alteration of the sample used in the present study, electron microprobe analyses of the formerly pure biotite grains are intermediate between fresh biotite and chlorite. Therefore, the average biotite composition of an unaltered rock that was sampled from the same outcrop is reported in Table 1. The average composition of the chlorite that replaces the biotite was determined from the microprobe analysis to be $(Fe_{7.12}Mn_{0.14}Ti_{0.03}Mg_{1.8}Al_{2.72})(Si_{5.47}Al_{2.53})O_{20}(OH)_{16}$. As a result of the heterogeneity of the sample, it is not possible to use the results of the electron microprobe analyses to estimate the degree of chloritization of the biotite. This and the relative abundances of the other minerals are discussed in section 5.1 below.

Owing to the relatively large grain size of the mineral separates, many grains were composed of more than one mineral and so the fractions were not pure. The plagioclase-rich fraction contained a significant amount of perthitic alkali feldspar and some quartz.

Table 1. Concentrations of oxides (wt%) and formulas of major minerals in Elat Granite.

	SiO_2	TiO_2	Al_2O_3	FeO	MgO	CaO	Na_2O	K_2O	MnO	Mineral formula	Source[a]
Oligoclase	64.6		21.6	0.10		2.7	8.8	0.5		$Na_{0.76}K_{0.03}Ca_{0.13}Al_{1.14}Si_{2.88}O_8$	1
Albite										$NaAlSi_3O_8$	2
Microcline										$KAlSi_3O_8$	2
Biotite	34.2	2.9	18.2	27.5	3.9	0.07	0.2	9.5	0.5	$K_{1.9}Na_{0.05}Ca_{0.01}(Mg_{0.91}Fe_{3.6}Ti_{0.34}Mn_{0.07}Al_{0.71})Al_{2.65}Si_{5.35}O_{20}(OH,F)_4$	
Chlorite	23.2	0.2	18.8	36.1	5.1	0.06	0.2	0.1	0.7	$Fe_{7.12}Mn_{0.14}Ti_{0.03}Mg_{1.8}Al_{2.72})(Si_{5.47}Al_{2.53})O_{20}(OH)_{16}$	1

[a] Sources: 1, present study; 2, end-member composition; 3, Eyal et al., in press.

Table 2. Chemical composition (wt%) of Elat Granite and the mineral-rich fractions.

	Plagioclase rich fraction	Alkali feldspar–rich fraction	Bulk granite
SiO_2	66	65	76
Al_2O_3	20	19	14
FeO	0.22	0.11	1.6
TiO_2	0.01	0.01	0.12
CaO	1.62	0.29	0.96
MgO	0.03	0.01	0.20
MnO	0.01	0.01	0.03
Na_2O	7.4	3.3	4.0
K_2O	2.5	10	3.4
P_2O_5	0.04	0.02	0.06
Sum	97	99	101

The alkali feldspar-rich fraction contained some oligoclase and quartz. The biotite-rich fraction was composed mostly of biotite, which was partly replaced by chlorite. Table 2 shows the chemical composition of the bulk granite, the plagioclase-rich fraction and the alkali feldspar-rich fractions.

4.2. Dissolution Experiments

The variations of Al, Si, Na, K, Mg, Fe and Ca concentrations in the dissolution experiments with time are shown in Figure 1. Initially, the concentrations of some of the elements in each mineral-rich fraction increased with time, until they approached steady state (Figs. 1a,c,e). The concentrations of other elements generally decreased with time (Figs. 1b,d,f). The variations of the different elements with time in the bulk granite experiment (Figs. 1g,h) show greater fluctuations. In general, the concentrations of Si and Na increased with time, whereas those of Fe, Mg and K decreased with time.

5. DISCUSSION

5.1. Chemical and Mineralogical Composition of the Bulk Granite and the Mineral-Rich Fractions

To interpret the results of the dissolution experiments it is essential to determine the mineralogical composition of the bulk granite and the mineral separates. The altered sample that was used in the present study was initially studied using standard petrographic techniques. However, a petrographic analysis of a granite (or other coarse grain rock) is not a precise method for the following reasons: 1) a thin section does not represent the composition of a coarse grain rock; 2) it is hard to accurately estimate the concentration of minerals that are less abundant, such as biotite, or the degree of chloritization; and 3) one can not estimate the relative amount of plagioclase and K-feldspar in the perthitic alkali feldspar. The common practice in petrological studies is to use the chemical analysis of the rock and its constituent minerals to calculate a normative mineralogical composition. This procedure is straight-forward for fresh granite that contains only quartz, plagioclase, K-feldspars and biotite. However, as the altered sample also contains perthitic alkali feldspar and chlorite, the calculated normative mineralogy is not unique. Therefore, we used the composition of unaltered Elat Granite samples, taken from the same locality as

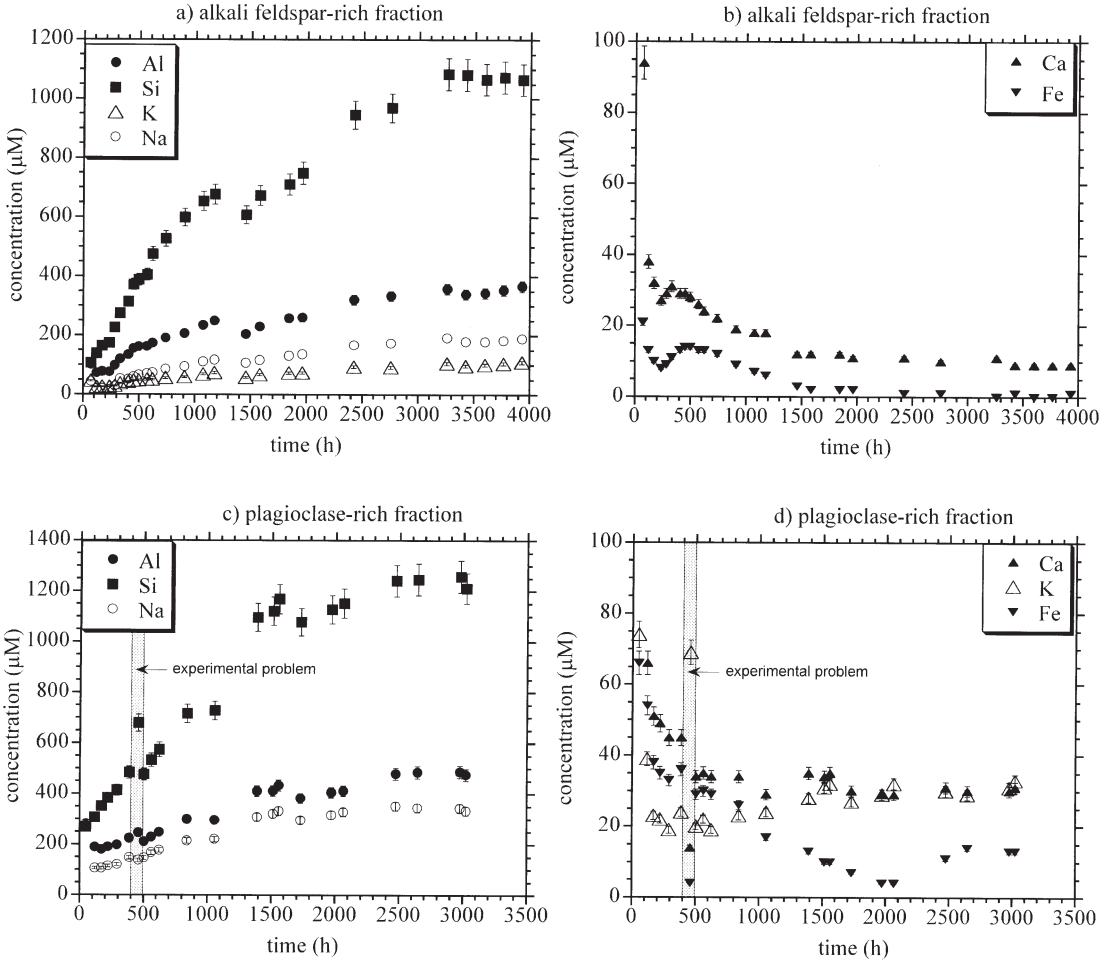

Fig. 1. Plot illustrating the variation of Al, Si, Na, K, Mg, Fe and Ca with time in the flow-through dissolution experiment of the alkali feldspar-rich fraction (a and b), plagioclase-rich fraction (c and d), biotite and chlorite-rich fraction (e and f) and the bulk granite sample (g and h).

the sample used in the present study, to constrain the calculated mineralogy. The unaltered samples show some variation in their chemical composition and modal mineralogical composition (Eyal et al., in press). As a first approximation we assume that the mineralogical composition of the hydrothermally altered Elat Granite is similar to that of unaltered granite with a similar chemical composition (Table 3). The major difference between the altered and unaltered samples is that the biotite in the altered rock is chloritized. In addition, the altered granite contains small amounts of sericite, clays and iron oxides. To estimate the amount of biotite and chlorite, as well as to determine the percentages of albite and microcline in the perthitic alkali feldspar, we use the chemical composition of the rock, which is given in Table 2.

The amount of biotite and chlorite is estimated based on the concentration of Mg in the bulk granite and the chemical composition of the biotite and the chlorite. Using the two alternate assumptions that all the Mg is either in chlorite or in biotite, the estimated percentages of these minerals range from 3.8 to 5.3%, respectively. Due to the large uncertainty associated with the electron microprobe determination of the mineral composition, the error in the above estimation is 15%–20%. The degree of chloritization may be estimated using the Ti concentration, as transformation of 2 mol of biotite to 1 mol of chlorite involves a significant decrease in the concentration of Ti, whereas the concentrations of Mg and Fe remain approximately constant (Table 1). Assuming that the Ti released during the transformation did not precipitate in secondary minerals, the concentration of Ti in the bulk granite was used to estimate the amount of biotite as 4.2%. The excess Mg was thereafter used to estimate the amount of chlorite (0.8%). Using this estimation the degree of chloritization is 15%. Taking into account an uncertainty of 20% in the estimation of Ti concentration of the biotite, the degree of chloritization is estimated to be between 0 to 30%. This range of values represents the minimum degree of chloritization, as it is possible that some of the Ti precipitated during the alteration.

The composition of the perthitic alkali feldspar in the bulk granite was calculated as follows. The amounts of Si, Al, Ca, Na and K in oligoclase ($Na_{0.76}K_{0.03}Ca_{0.13}Al_{1.14}Si_{2.88}O_8$) were calculated assuming that the rock contained 27% oligoclase, as was observed for the unaltered sample. The excess sodium was used to calculate the percentage of end-member albite (in perthitic alkali feldspar) in the sample (13.5%). The potassium

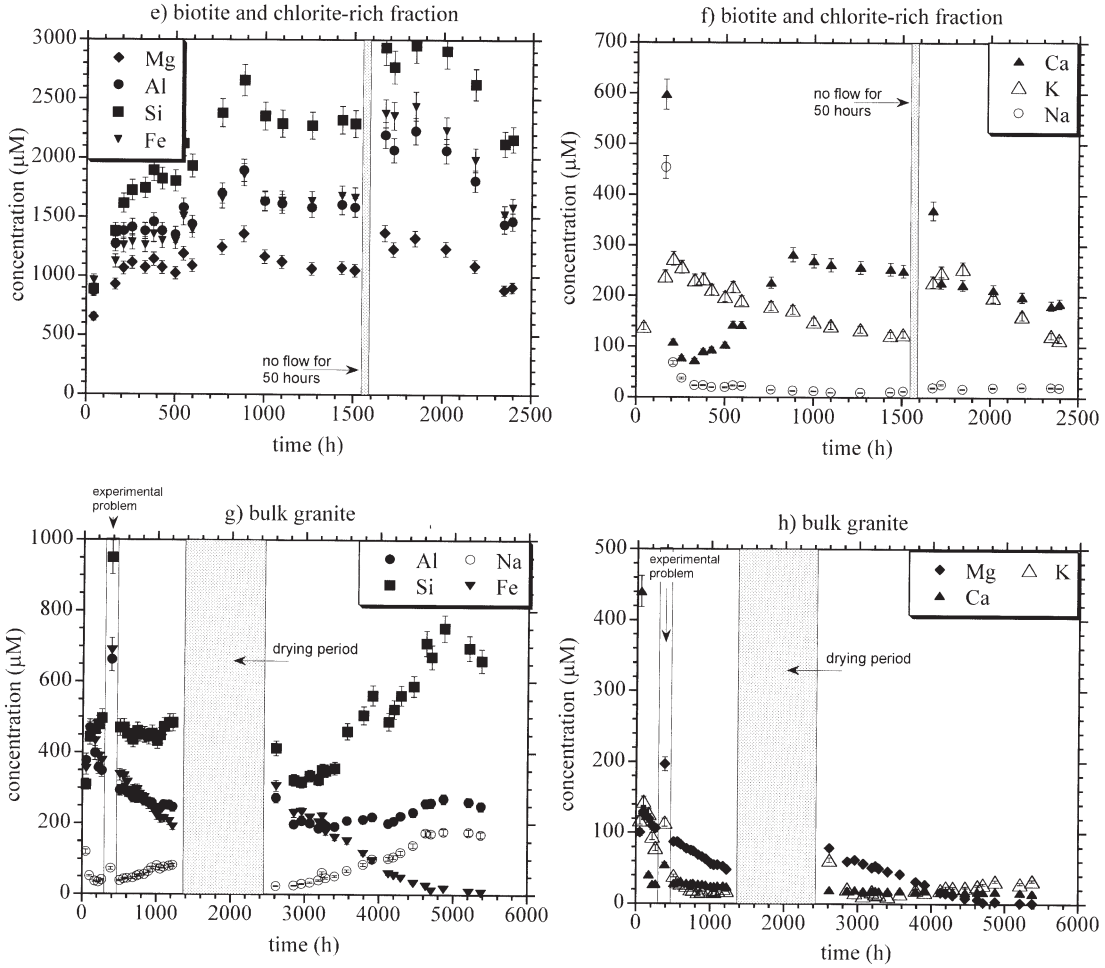

Fig. 1. (continued)

that was not used for the biotite and the oligoclase was used to calculate the percentage of end-member microcline (in perthitic alkali feldspar) in the sample (17.0%). The calculated total percentage of perthitic alkali feldspar (30.5%) is the same as the estimated amount of perthitic alkali feldspar in the unaltered sample (Table 3). The amount of quartz in the sample was estimated by assigning to quartz all the silicon that remains after constructing the biotite, the chlorite, the perthitic alkali feldspar and the oligoclase. The percentage of apatite (as $Ca_5(PO_4)_3(OH)$) was estimated based on the phosphate concentration. After these calculations a small unexplained amount of Fe, Ca and Al remained. The excess iron probably represents precipitation of secondary iron oxide (0.1%), and the Ca and Al (with some of the Si that was assigned as quartz) represent precipitation of secondary clay and some calcite. Alternatively, these small amounts of Ca and Al may be the result of accumulated uncertainties. The errors associated with the above determinations are in the range of 10%–20% of the estimated values. These errors are similar to the variability in the normative composition of unaltered Elat granites that were sampled from the same outcrop (Eyal et al., 2005).

The relative amounts of oligoclase in the plagioclase-rich and the alkali feldspar-rich fractions were estimated assuming

Table 3. Mineralogical composition (wt%) of Elat Granite and the mineral-rich fractions.

	Unaltered Eilat Granite	Bulk granite	Plagioclase rich fraction	Alkali feldspar–rich fraction
Quartz	37.5	37.3	6.7	6.5
Oligoclase	27	27	60	11
Albite in perthitic alkali feldspar	nd[a]	13.5	19	20
Microcline in perthitic alkali feldspar	nd	17	13.4	59
Total perthite	30.5	30.5	32.4	79
Biotite	4.8	4.2	<1	<0.5
Chlorite	none	0.8		
Apatite	nd	0.2	<0.1	<0.1
Source[b]	2	1	1	1

[a] nd = not determined.
[b] Sources: 1, present study (see section 5.1); 2, normative calculation; 3, Eyal et al., in press.

that all the Ca is in oligoclase. The amounts of albite and microcline in perthitic alkali feldspar and the amount of quartz were estimated by applying the same method that was used to construct the composition of the bulk granite. The results of the calculations are shown in Table 3. The calculated microcline / albite ratio of the perthitic alkali feldspar in the bulk granite (1.3) is intermediate between that of the plagioclase-rich fraction (0.7) and the alkali feldspar-rich fraction (3.0). These differences in compositions are expected as microcline / albite ratio is not constant in the perthitic alkali feldspar grains, and during gravimetric mineral separation the plagioclase-rich fraction would be enriched with grains that contain more albite, whereas the alkali feldspar-rich fraction would be enriched with grains that contain more microcline.

5.2. The Release Rate of Major Elements from the Plagioclase- and Alkali Feldspar-Rich Fractions

Based on the changes in concentrations with time (Fig. 1), the instantaneous release rate of the different elements in each of the experiments was calculated using Eqn. 2. The release rates of Na and K from the plagioclase-rich and the alkali feldspar-rich fractions (Fig. 2a) are used to estimate the change in dissolution rate of oligoclase, albite and microcline with time. The calculations are based on the following assumptions: 1) The dissolution of the three feldspars is stoichiometric. 2) The dissolution rates of the oligoclase and the albitic phase in the perthitic alkali feldspar are the same. Although the dissolution of Ca-feldspar is faster than that of Na-feldspar, this assumption is reasonable as the difference between the dissolution rate of end member albite and An_{20} is less than the uncertainty (Blum and Stillings, 1995). 3) The release of Na and K in the plagioclase-rich and the alkali feldspar-rich fractions are solely due to the dissolution of oligoclase and perthitic alkali feldspar, and therefore:

$$Rate_{Na} = Rate_{plag} \cdot \nu^{Na}_{oligo} \cdot m_{oligo} + Rate_{plag} \cdot \nu^{Na}_{ab} \cdot m_{ab} \quad (6)$$

$$Rate_{K} = Rate_{plag} \cdot \nu^{K}_{oligo} \cdot m_{oligo} + Rate_{micro} \cdot \nu^{K}_{micro} \cdot m_{micro} \quad (7)$$

where $Rate_{plag}$ is the dissolution rate (mol g^{-1} s^{-1}) of the oligoclase and albite and $Rate_{micro}$ is that of the microcline, ν^{i}_{j} is the stoichiometric coefficient of element i in mineral j (Table 1) and m_j (g) is the mass of mineral j in the fraction. The common practice in experimental kinetics is to normalize the dissolution rate to the total surface area of the pure mineral, which is measured by the Brunauer-Emmett-Teller (BET) method, (Brunauer et al., 1938). In the present study we could not measure the surface area of an individual mineral in the mixtures and therefore we normalized the dissolution rates by the mass of the minerals. The dissolution rates of the plagioclase and microcline were calculated by rearranging Eqns. 6 and 7, respectively:

$$Rate_{plag} = \frac{Rate_{Na}}{\left(\nu^{Na}_{oligo} \cdot m_{oligo} + \nu^{Na}_{ab} \cdot m_{ab}\right)} \quad (8)$$

$$Rate_{micro} = \frac{Rate_{K} - Rate_{plag} \cdot \nu^{K}_{oligo} \cdot m_{oligo}}{\nu^{K}_{micro} \cdot m_{micro}} \quad (9)$$

The initial mass of the dissolving minerals in each fraction was calculated from the product of the starting mass of the fraction and the estimated percentage of the mineral in the fraction (Table 3). Following each stage (i.e., the time between the replacements of two sequential output bottles), the remaining mass of each mineral was updated based on its dissolution rate and the duration of the stage. As not all the samples were analyzed, missing values were interpolated assuming linear change with time between the previous and the following sample.

The calculated plagioclase and microcline dissolution rates during the experiments were determined independently for the dissolution experiments of the plagioclase-rich and the alkali feldspar-rich fractions (Fig. 2b). There is an excellent agreement between the two independent estimates of the dissolution rates. As the release rates of Na and K and the percentage of the minerals in the fractions were determined independently for the plagioclase-rich

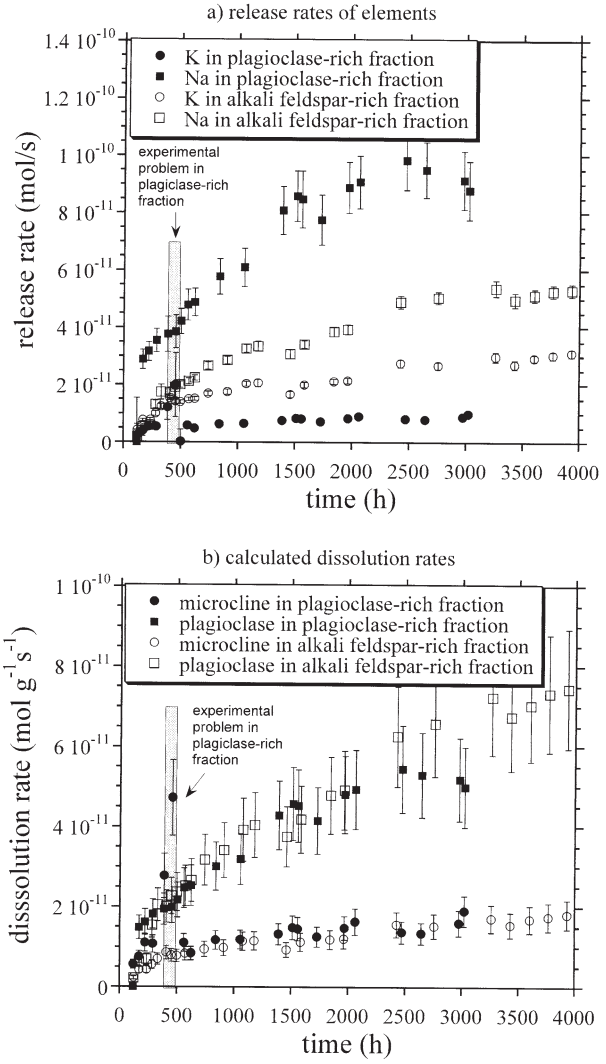

Fig. 2. (a) The release rates of Na and K with time in the dissolution experiments of the plagioclase-rich and the alkali feldspar-rich fractions. The release rates of both elements were different in the two experiments. (b) Dissolution rates of plagioclase and microcline, which were calculated based on the release rates of Na and K, are highly consistent during the course of the two experiments (see section 5.2).

and the alkali feldspar-rich fractions, the strong agreement between the estimates of the change in dissolution rates with time supports both the obtained dissolution rates and the estimates of the mineralogical compositions of the fractions. Based on the results of the two experiments, the steady state dissolution rates of plagioclase and microcline are estimated to be 6.2 ± 1.2 $\times 10^{-11}$ mol g^{-1} s^{-1} and 1.6 ± >0.3 $\times 10^{-11}$ mol g^{-1} s^{-1}, respectively.

Chou and Wollast (1984) measured the dissolution rate of albite in pH 1.2 to 5.1. Extrapolating the rate data of Chou and Wollast (1984) to pH 1 yields an albite dissolution rate of 1 $\times 10^{-10}$ mol m^{-2} s^{-1}. For microcline, Schweda (1989) reported a dissolution rate of 3 $\times 10^{-11}$ mol m^{-2} s^{-1} at pH 1. To compare the present study rates to those reported in the literature, we calculated the average geometric surface area of the feldspars using a spherical geometry and a density of 2.65 g/cm^3, to be 0.02 m^2 g^{-1}. The obtained dissolution rates for plagioclase (3 $\times 10^{-9}$ mol m^{-2} s^{-1}) and microcline (8 $\times 10^{-10}$ mol m^{-2} s^{-1}) are 31 and 27 times faster than the respective literature rates. However, this comparison is problematic as Chou and Wollast (1984) and Schweda (1989) normalized their rates to BET surface area, which due to surface roughness is typically much larger than geometric surface area. According to White and Brantley (2003) the surface roughness of feldspar ranges between 5 and few hundreds, and it is in average 9.2 and 8.4 for plagioclase and K-feldspar, respectively. Recalculating our rates using these average values yields dissolution rates of 3.3 $\times 10^{-10}$ and 9.5 $\times 10^{-11}$ mol m^{-2} s^{-1} for plagioclase and microcline, respectively. These rates are ~3 times faster than rates reported in the literature. This difference in rates may be explained by high roughness of the minerals used in the present study due to the presence of many microcracks.

Using the obtained changes in the dissolution rates of plagioclase and microcline with time, the release rates ($Rate_i$) of any element, i, which composes these minerals, may be predicted using the equation:

$$Rate_i = Rate_{plag} \cdot \nu^i_{oligo} \cdot m_{oligo} + Rate_{plag} \cdot \nu^i_{ab} \cdot m_{ab} + Rate_{micro} \cdot \nu^i_{micro} \cdot m_{micro} \quad (10)$$

Figure 3 compares the measured release rates of Al, Si and Ca during the experiment to the predicted values that were calculated using Eqn. 10. For Al and Si there is a good agreement between the predictions and the actual release rates throughout the duration of the experiments (Figs. 3a,b). This good agreement is an additional support for the estimations of the dissolution rates. The release rate of Ca, in contrast to that of K, Na, Al and Si, was initially rapid but it decreased with time. Towards the end of the experiments the release rate of Ca was equal within error to the release rate predicted based on the dissolution rate of the plagioclase and the stoichiometry of Ca in plagioclase (Fig. 3c). The initially rapid release of Ca is probably the result of release from other rapidly dissolving minerals such as calcite and apatite as well as from exchangeable sites in clays. The role of calcite in the chemical weathering of granitoid rocks was discussed in previous studies (e.g., White et al., 1999, and references therein), and is further discussed in Erel et al. (2004).

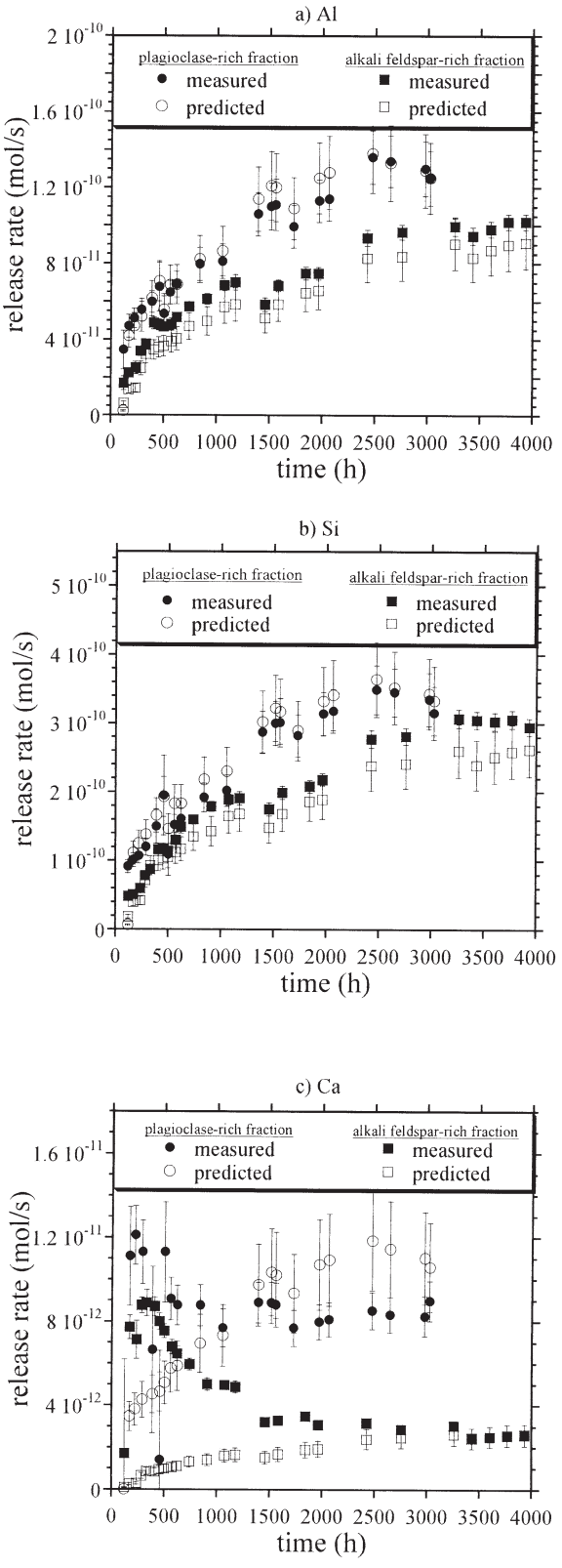

Fig. 3. Comparison of the measured release rates of (a) Al, (b) Si and (c) Ca during the course of the dissolution experiments of the plagioclase- and the alkali feldspar-rich fractions, with the predicted values that were calculated based on the dissolution rates of plagioclase and microcline assuming stoichiometric dissolution (see section 5.2).

5.3. The Effect of Iron Coating on the Dissolution Rate of Plagioclase

In both the plagioclase-rich fraction and the alkali feldspar-rich fraction the concentrations of the major elements increase with time (Figs. 1a,c). This increase is interpreted as the result of a significant enhancement with time of the plagioclase dissolution rate (Fig. 2b). It is interesting to note that the increase in plagioclase dissolution with time was also accompanied by changes in the $^{206}Pb/^{207}Pb$ ratio released during the dissolution of these fractions (Erel et al., 2004). Such an enhancement in rate is not typical of laboratory dissolution experiments. In most cases mineral dissolution rates decrease with time as a result of the extinction of highly reactive fine particles (e.g., Helgeson et al., 1984) and of the decrease in the ratio of reactive to unreactive sites (e.g., Gautier et al., 2001). We suggest that the increase in plagioclase dissolution rate observed in the present study is explained by progressive exposure of plagioclase surface sites due to the removal of iron oxide coatings. These coatings appear both on the external surface of the grains and in microscopic cracks that cut through the grains. As a result, many of the new surfaces that were formed by grinding are also coated. Most of the iron was released to solution during the first 2000 h of the experiments (Figs. 1b,d), and thereafter the plagioclase dissolution rate approached a steady state (Fig. 2b). Note that only part of the iron in the sample was dissolved during the first 2000 of the experiment. However, the observation that the release rate of iron after this period was slow indicates that the rest of the iron is in microscopic cracks that were not exposed to solution. Alternatively, the increase of plagioclase dissolution rates may be explained by an increase in the surface roughness of the plagioclase due to its dissolution. As we did not determine the reactive surface area of the plagioclase, we can not reject this possibility. However, as will be shown below there is a strong linear relation between the dissolution of the exposed iron coating and the increase in the plagioclase dissolution rate, and therefore it seems more reasonable that the enhancement in dissolution rate is the result of the removal of the iron oxide coating.

To determine the effect of the iron coatings on the plagioclase dissolution rate, we first estimated the change in abundance of iron coatings on external surfaces of plagioclase in each of the experiments. As the experiment using the alkali feldspar-rich-fraction was longer than that with plagioclase-rich fraction, we did not use the data from the last 1000 h of the former experiment. The amount of iron that was released during this period was minimal (Fig. 1b) and therefore, the result of the calculation is not influenced by excluding these data. In the calculation we assume that all of the iron that was released during each experiment (47 and 17 μmol in the experiment with plagioclase-rich and alkali feldspar-rich fractions, respectively) was from coatings that were evenly distributed on the external surfaces of the oligoclase and on the albitic phase in the perthitic alkali feldspar. Therefore, the initial amount of iron coating was 19 and 16 μmol/g of oligoclase and albite in the plagioclase-rich and alkali feldspar-rich fractions, respectively. The similarity in the estimated amount of iron coating on oligoclase and albite in the two fractions supports the assumption that the iron coating is mainly associated with the oligoclase and the albite. The amount of remaining iron coating during each experiment was calculated by subtracting the amount of iron released with time from the initial amount. As not all of the samples were analyzed, missing values were interpolated assuming linear change with time between the previous and the following sample. Figure 4 shows that the plagioclase dissolution rate increases almost linearly (R^2 of 0.94 and 0.90 in the experiment with the plagioclase- and the alkali feldspars-rich fractions, respectively) as a result of the removal of the iron coating. Again, there is a very good agreement between the two experiments.

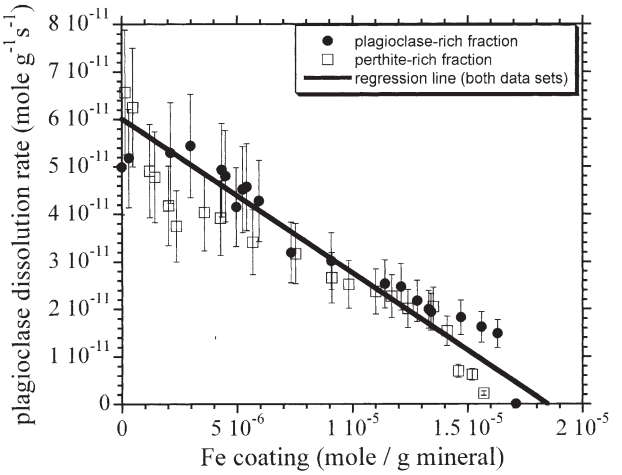

Fig. 4. The effect of iron coating on plagioclase dissolution rate.

5.4. The Release Rates of Major Elements from the Biotite and Chlorite-Rich Fraction

In contrast to the plagioclase- and alkali feldspar-rich fractions, dissolution of the biotite and chlorite-rich fraction is clearly non-congruent. Figure 5 compares the ratio of the release rates of different elements to their molar ratio in the biotite and chlorite. Although some of the ratios are intermediate between the stoichiometric ratios of the chlorite and those of the biotite, they cannot reflect a combined effect of congruent dissolution of biotite and chlorite, as they do not represent the same mixing ratio. For example, the Al/Si and Fe/Si ratios (Figs. 5a,b) reflect the dominance of biotite dissolution whereas K/Si and Mn/Si (Figs. 5c,d) reflect the dominance of chlorite dissolution. Other release ratios (e.g., Mg/Si and Mg/Fe) are significantly higher than the stoichiometric ratios of both the biotite and the chlorite (Figs. 5e,f). Non-stoichiometric dissolution of chlorite and biotite is commonly observed in dissolution experiments (e.g., Afifi et al., 1985; Acker and Bricker, 1992; Malmstrom and Banwart, 1997; Taylor et al., 2000; Brandt et al., 2003), and may reflect several processes: 1) dissolution of a third phase; 2) selective dissolution of different elements from the biotite and / or the chlorite surfaces; and 3) precipitation of one or more secondary phases. The observation that the Mg/Fe ratio at steady state is above 0.6 (higher than that of both the biotite and the chlorite; Fig. 5f) rules out the first possibility, as the system does not contain any phase with

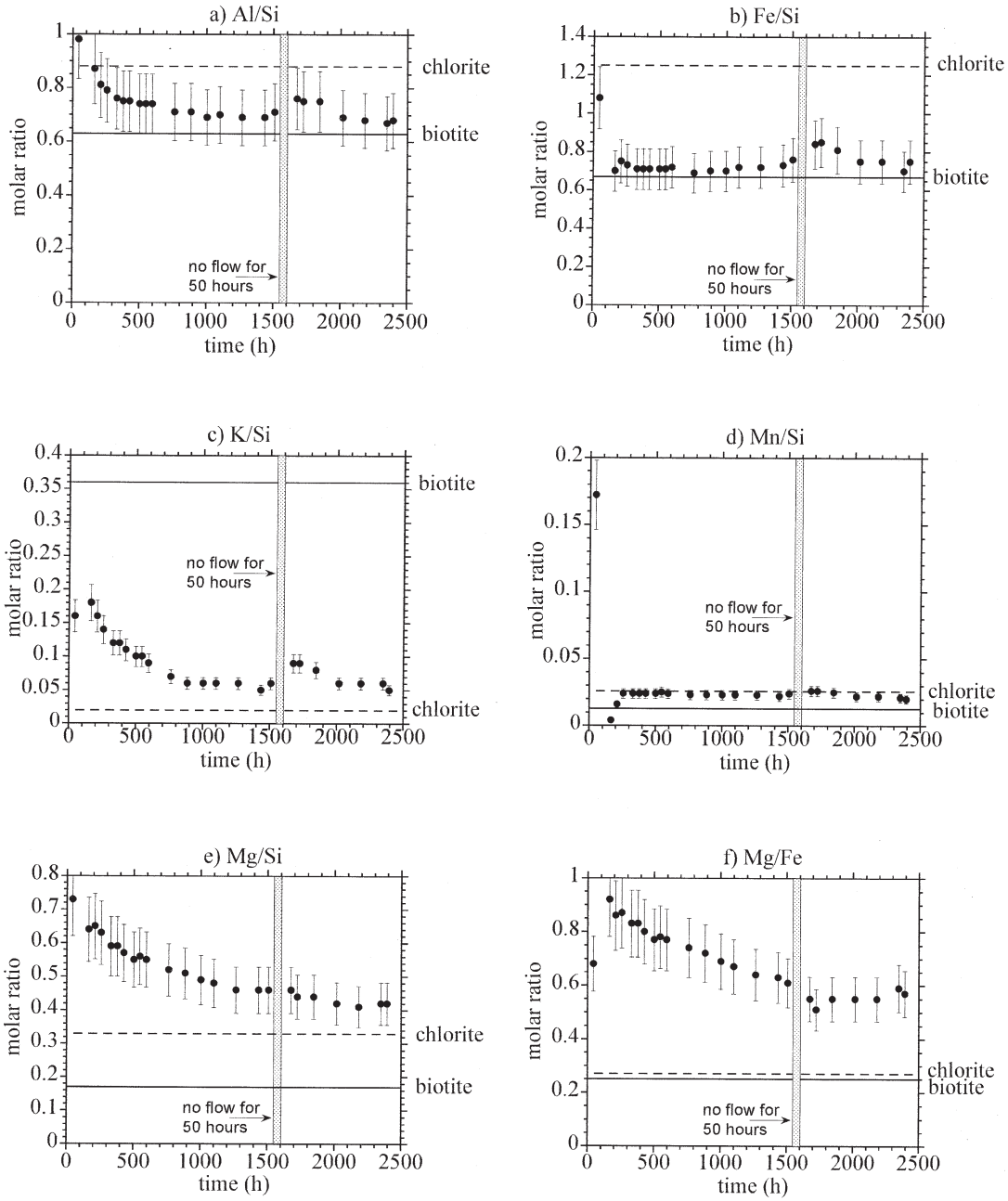

Fig. 5. Comparison of the ratio of the release rates of (a) Al/Si; (b) Fe/Si; (c) K/Si; (d) Mn/Si; (e) Mg/Si; and (f) Mg/Fe during the course of the dissolution of the biotite and chlorite-rich fraction (closed circles) to the stoichiometric ratios of biotite and chlorite (horizontal lines).

Mg/Fe ratio >0.6. The observation that dissolution remains incongruent throughout the experiment (2400 h), indicates that the long-term non-stoichiometric dissolution is not a result of selective dissolution.

We suggest that the release rate of the different elements in the biotite and chlorite-rich fraction is controlled by the dissolution of biotite and chlorite and precipitation of nontronite ($X_{0.3}Fe_2(Si,Al)_4O_{10}(OH)_2 \cdot n(H_2O)$, where X is a cation in an interlayer site). Precipitation of clay associated with biotite dissolution was also observed in the granite dissolution experiments of Afifi et al. (1985). Saturation indexes (SI) calculated using the EQ3NR code (Wolery, 1992) indicate that throughout the dissolution experiment of the biotite and chlorite-rich fraction, the solution was saturated or supersaturated with respect to nontronite and several SiO_2 phases (quartz, chalcedony, amorphous silica, tridmite, cristobalite and coesite). The observation that the solution is saturated with respect to a specific phase is an indication that the phase may have been precipitated, but does not prove that it was actually precipitated. Unfortunately, it is not possible to identify small amounts of nontronite using XRD. Supporting evidence for the precipitation of nontronite comes from a mass-balance calculation. The

calculation was based on the assumptions that the biotite and / or the chlorite dissolved congruently and that all of the Mg remained in solution, i.e., that the secondary phases did not contain any Mg. The rate of precipitation of Si, Al, Fe and K (P_Rate_i, mol element s^{-1}) was calculated from the equation:

$$P\_Rate_i = Rate_{Mg}\left(Frac_{Bio}\cdot \nu^i_{Bio}/\nu^{Mg}_{Bio} + \left(1-Frac_{Bio}\right)\cdot \nu^i_{Chl}/\nu^{Mg}_{Chl}\right) - Rate_i \quad (11)$$

where $Rate_i$ is the release rate (mol s^{-1}) of an element i that was calculated using Eqn. 2, ν^i_j is the stoichiometric coefficient of element i in mineral j (Table 1) and $Frac_{Bio}$ is the fraction of the release rate of Mg that is a result of biotite dissolution. Precipitation rates of Si, Al, Fe and K were calculated for two end-member cases, the first in which only biotite is dissolved ($Frac_{Bio} = 1$) and the second in which only chlorite is dissolved ($Frac_{Bio} = 0$). The average Al/Si, Fe/Si and K/Si ratios for the case in which biotite controls the dissolution rate are 0.58 ± 0.02, 0.64 ± 0.03 and 0.50 ± 0.05, respectively (the ± represents the standard deviation of the average). For the second case, the average Al/Si and Fe/Si ratios are 1.5 ± 0.3 and 2.5 ± 0.5, respectively. The composition of the octahedral and tetrahedral sites of possible precipitated phases were calculated from the average Al/Si and Fe/Si ratios using a general formula of a dioctahedral smectite $X_xY_2Z_4O_{10}(OH)_2$, where Y is an octahedral site, Z is a tetrahedral site, and X is an interlayer site. For the case in which biotite controls the dissolution rate, the resulting composition is $X_{1.3}(Fe_{1.7}Al_{0.3})(Si_{2.7}Al_{1.3})O_{10}(OH)_2$, which is an intermediate composition on the nontronite-beidellite solid solution (85% nontronite). For the case in which chlorite controls the dissolution rate, the calculated composition of the precipitated phase is $X_3(Fe_2)(Si_{1.2}Al_{1.8}Fe_{1.0})O_{10}(OH)_2$. Although Fe^{+3} may occupy the tetrahedral site in nontronite (Gaines et al., 1997), the small amount of Si in the tetrahedral site and the resulting large amount of interlayer cations (3) make the precipitation of such a phase less reasonable. Based on both thermodynamic and mass balance calculations, we propose that the best explanation for the non-congruent dissolution of the biotite and chlorite-rich fraction is dissolution of (mainly) biotite and precipitation of nontronite. This explanation is in accordance with the values of $^{87}Sr/^{86}Sr$ released during the dissolution of the biotite and chlorite-rich fraction which indicate a preferential dissolution of the interlayer sites relative to the framework sites (Erel et al., 2004). This is because of the fact that $^{87}Sr/^{86}Sr$ values should reflect only the dissolution of biotite and are not sensitive to the precipitation of any secondary phase.

The amount of biotite that was dissolved during the experiment was calculated based on the amount of Mg that was released to the solution, assuming that the fraction is composed solely of biotite. As not all the samples were analyzed, missing values were interpolated assuming linear change with time between the previous and the subsequent samples. According to this calculation more than 85% of the biotite was dissolved during the experiments. A similar calculation assuming that the fraction is composed solely of chlorite indicates a loss of more than 60% of the chlorite. As the (non steady-state) release rate of Mg remains approximately constant despite the significant loss of the dissolving mineral, we suggest that dissolution of the biotite/chlorite-rich fraction occurred under near-equilibrium conditions with respect to the dissolving phase (mostly biotite), and therefore the release rate of Mg remained constant although the amount of available surface area decreased with time. As we do not know the relative amounts of biotite and chlorite in the biotite and chlorite-rich fraction, nor the proportion of Mg that is derived from biotite, it is not possible to determine the actual dissolution rate of biotite and chlorite. As a first approximation it is possible to calculate the rate for two end-member cases, one in which the sample is composed solely of biotite and the other in which it is composed of chlorite. The change with time of biotite and chlorite dissolution rate for these case studies is shown in Figure 6. Due to the uncertainty in the initial amount of the biotite, the relative uncertainty in the amount of biotite that is left in the system increases as most of the biotite is dissolved. After ~2000 h this uncertainty is of the order of the estimated value. Therefore, only the rates calculated during the first 1500 h are used for the comparison with the bulk granite experiment.

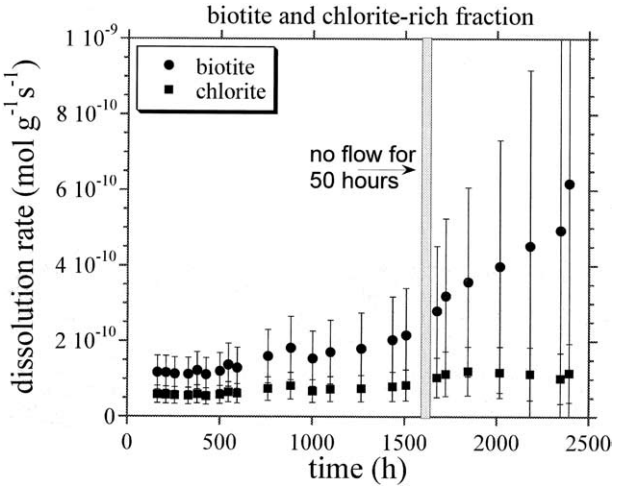

Fig. 6. The change with time of biotite and chlorite dissolution rate during the dissolution of the biotite and chlorite-rich fraction, which was calculated assuming that the sample is composed solely of biotite or chlorite, respectively (see section 5.4).

5.5. Comparison of the Release Rate of the Major Elements from the Bulk Granite to the Dissolution Rates of Its Constituent Minerals

The release rates of the major elements during the dissolution of the bulk granite are controlled by the dissolution rate of plagioclase (Na, Al and Si), microcline (K, Al and Si) and biotite /chlorite (Mg, Fe, K, Al and Si). The release rates of Mg and Na are controlled by the dissolution rate of biotite and plagioclase, respectively, and therefore the relative release rate of these two elements (Fig. 7a) can be used to examine the relative dissolution rate of biotite and plagioclase during the dissolution of granite. Initially, biotite/chlorite dissolution dominates, but with time, a transition from biotite + chlorite-dominance to plagioclase control on the release of elements from the granite is observed. As a result of the drying, the rate of biotite dissolution increased significantly (the release rate of Mg was almost doubled) while that of plagioclase decreased

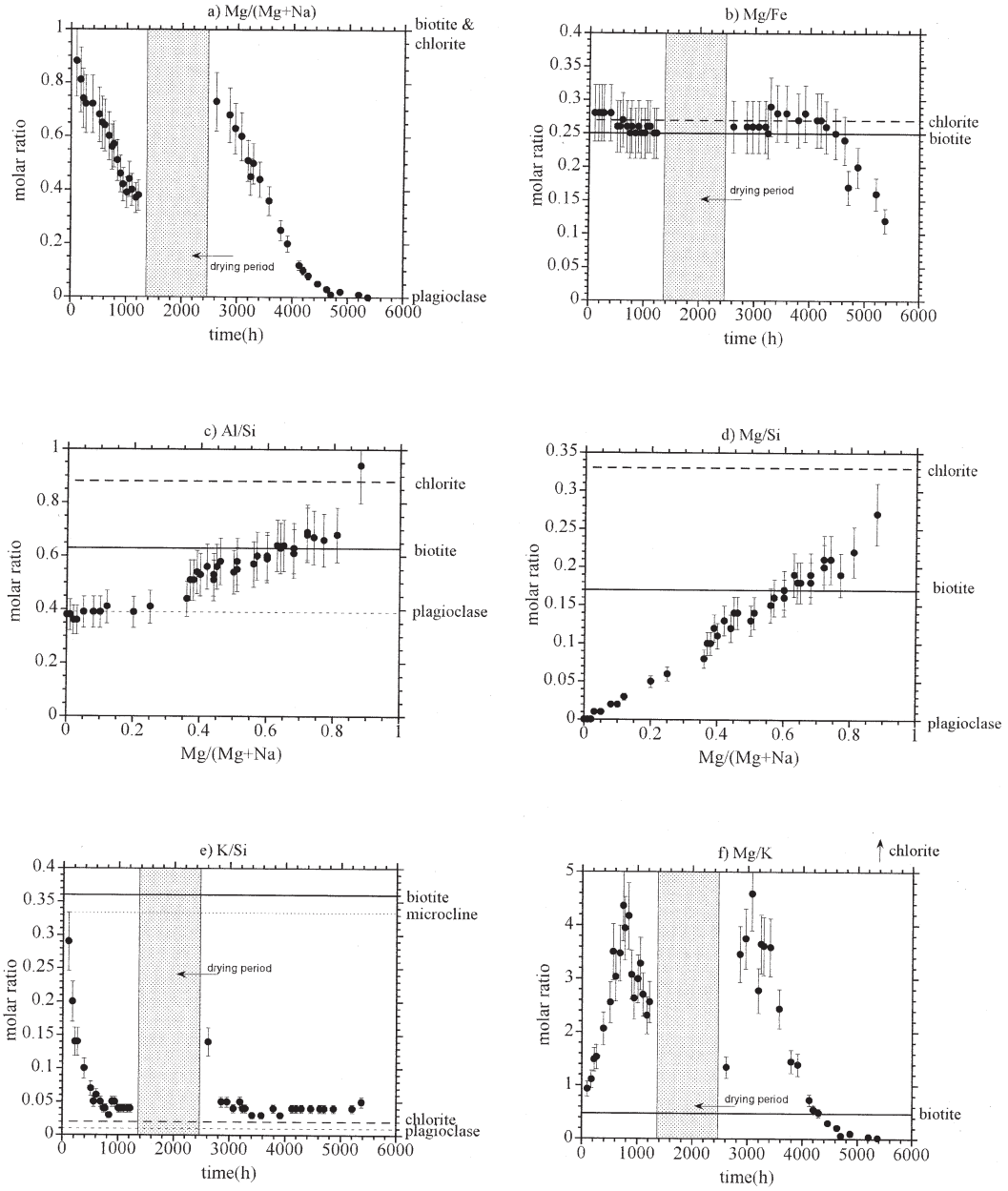

Fig. 7. Comparison of the ratio of the release rates of (a) Mg/(Mg + Na); (b) Mg/Fe; (c) Al/Si; (d) Mg/Si; (e) K/Si; and (f) Mg/K during the dissolution of the bulk granite (closed circles) to the stoichiometric ratio in its constituent minerals (horizontal lines).

(the release rate of Na reduced to half), and biotite dissolution dominated again. Thereafter, the transition to plagioclase dominance recurred, until the biotite and chlorite had dissolved completely. These stages in the granite dissolution were also documented by changes in the $^{206}Pb/^{207}Pb$ and $^{87}Sr/^{86}Sr$ ratios (Erel et al., 2004).

In contrast to the non-stoichiometric dissolution of the biotite/chlorite-rich fraction (Fig. 5), the release of major elements within the tetrahedral and octahedral sites of biotite and chlorite (Al, Si Mg and Fe) indicates that these minerals dissolved stoichiometrically during the dissolution of the bulk granite. The ratio of the release rate of Mg/Fe from the bulk granite is equal to the stoichiometric ratio of the biotite and chlorite (Fig. 7b). Similarly, the ratios of the release rate of Al/Si and Mg/Si are equal to the stoichiometric ratio of the biotite and chlorite during the periods in which the dissolution of these minerals is dominant (the first few hundreds of hours of the experiments and following the resumption of the experiment after the drying period, (Figs. 7c,d). Both Al/Si and Mg/Si ratios show that dissolution of chlorite makes a greater contribution (i.e., higher ratios) at the onset of the experiment.

In common with Mg, the release of K from the bulk granite (Fig. 1h) is initially rapid and it decreases with time. Following the drying period, the K concentration increases and then

decreases again. Both the initial decrease in K concentration and the decrease following the drying period are at a greater rate than the parallel decrease in Mg concentration (Fig. 1h). We suggest that the faster decrease in K concentration indicates that the release rate of ions from interlayer sites in biotite is faster than that from the tetrahedral and octahedral sites that build the biotite framework. This suggestion is also supported by fast changes in $^{87}Sr/^{86}Sr$ ratios (Erel et al., 2004). The observations that the release ratio of Mg/K is always higher and K/Si is always lower than the stoichiometric ratios of biotite (Figs. 7e,f) are explained by the high contribution of chlorite during the initial period of dissolution in which the K is released from the interlayer of the biotite.

The change with time in the mass of biotite in the bulk granite was calculated based on the amount of Mg that was released to the solution, assuming that the sample contained no chlorite and that the original percentage of biotite in the bulk granite was 5.3 ± 1 (see section 5.1 above). In contrast to the observations in the biotite/chlorite-rich fraction, the release rate of Mg from the bulk granite decreased linearly with the estimated decrease in the biotite mass, except following the drying interval. A similar trend was obtained when we calculated the remaining mass of chlorite, assuming that the bulk granite contained no biotite. The concentrations of the major elements during the dissolution of the bulk granite were relatively low, and the dissolution of biotite (and/or chlorite) from the bulk granite occurred under far from equilibrium conditions, and therefore the release rate of the magnesium is proportional to the amount of biotite and chlorite available for dissolution.

Figure 8a compares the calculated biotite dissolution rate in the bulk granite dissolution experiment to that in the dissolution experiment of the biotite/chlorite-rich fraction. During the first 600 h of the experiments the dissolution rate of biotite in the experiment with the biotite/chlorite-rich fraction is significantly slower than that in the bulk granite. The observed slower biotite dissolution rate in the former experiment supports our suggestion that the dissolution of the biotite/chlorite-rich fraction occurred under near-equilibrium conditions with respect to the dissolving phase. As the experiments progress, the uncertainty of the calculated dissolution rates becomes larger than the calculated differences due to the increase in the relative uncertainty of the estimation of the biotite mass.

The release rate of Na and K at steady state was calculated using Eqn. 4. The masses of oligoclase, albite and microcline in the bulk granite at steady state were calculated based on the amounts of Na and K that were released to the solution, using a method similar to the one used to calculate the changes in mass in the plagioclase- and alkali feldspar-rich fractions. As some of the K is released from biotite, the release of K was neglected in samples that had a ratio of Mg/(Na + Mg) higher than 0.6. According to this calculation the final mass of the oligoclase and albite was reduced to 89%, and that of microcline to 96%, of their original estimated mass. The dissolution rates of plagioclase and microcline at steady state were calculated from the above estimations of the release rate of Na and K and the final mass of the minerals using Eqns. 8 and 9, respectively. The obtained steady state dissolution rates of plagioclase ($6.6 \pm 1.3 \times 10^{-11}$ mol g^{-1} s^{-1}) and microcline ($1.9 \pm 0.4 \times 10^{-11}$ mol g^{-1} s^{-1}) show excellent agreement with the average steady state rates obtained from the plagio-

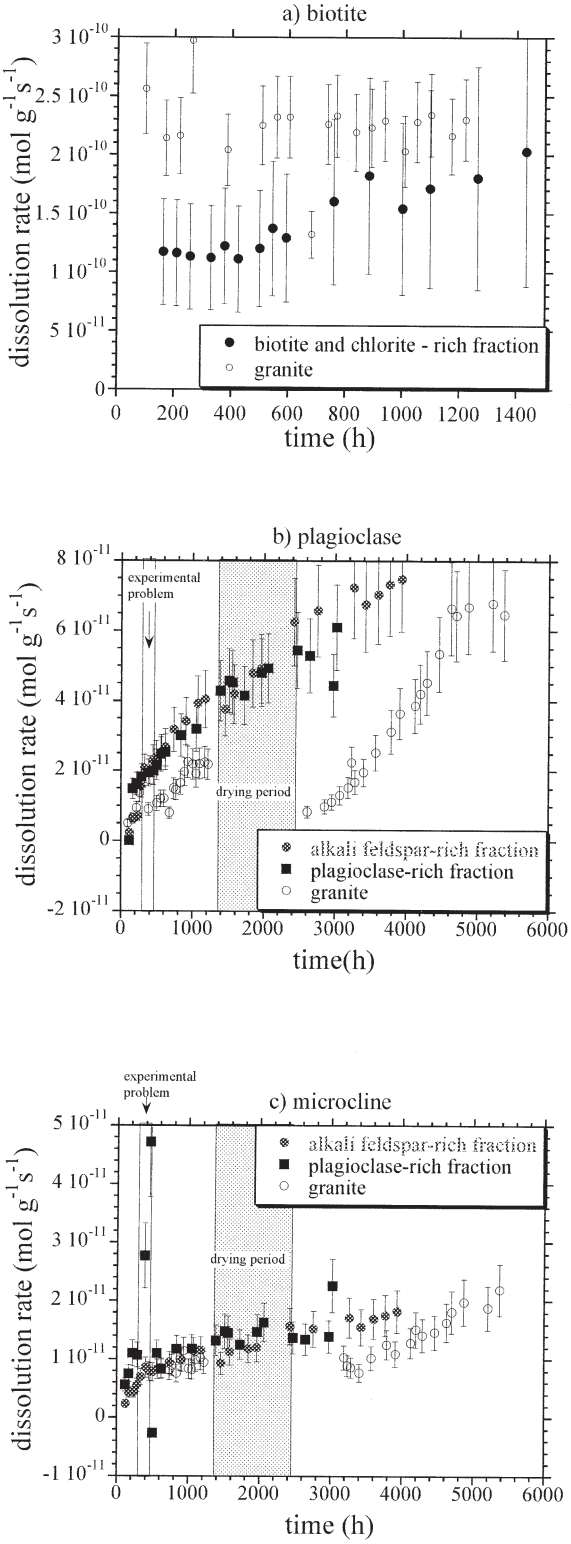

Fig. 8. Comparison of the calculated dissolution rates of (a) biotite, (b) plagioclase and (c) microcline during the dissolution of the bulk granite to those rates during the experiments with the mineral-rich fractions.

clase- and alkali feldspar-rich fractions ($6.2 \pm 1.2 \times 10^{-11}$ and $1.6 \pm 0.3 \times 10^{-11}$ mol g^{-1} s^{-1}, for plagioclase and microcline, respectively). The dissolution rate of microcline was calculated only for samples that show small effects of biotite dissolution (e.g., Mg/(Na + Mg) < 0.6). Figures 8b and c compare the calculated plagioclase and microcline dissolution rates in the bulk granite dissolution experiment to those rates in the dissolution experiment of the plagioclase- and alkali feldspar-rich fractions. Until the drying period, there is a very good agreement between the three estimates of the microcline dissolution rate. In contrast, the dissolution rates of plagioclase in the experiment with the plagioclase- and the alkali feldspar-rich fraction are significantly faster than that in the bulk granite. As we showed above, the dissolution rate of the plagioclase is initially inhibited by the Fe coating. As a result of biotite dissolution, the iron concentration in solution during the first 1000 h of the experiment with the bulk granite (Fig. 1g) was about an order of magnitude higher than that in the experiment with the plagioclase-rich fraction (Fig. 1d). We suggest that the dissolution rate of the iron coating in the bulk granite experiment was slower due to the higher Fe concentration, and as a result the increase in plagioclase dissolution rate was initially slower.

5.6. Implications of the Present Study to the Comparison between Dissolution Rate in the Laboratory and in the Field

The amount of biotite and chlorite in the biotite/chlorite-rich fraction was ~20 times higher than that in the bulk granite experiment. As a result, concentrations of major elements were higher in the former experiment, and the solution became supersaturated with respect to a secondary mineral (nontronite) and close to equilibrium with respect to biotite (and or chlorite) dissolution. Consequently, the biotite/chlorite-rich fraction dissolved slower than the biotite and chlorite in the bulk granite and did so non-stoichiometrically. The instantaneous water/rock ratio in the field is limited by porosity and is orders of magnitude lower than that in any well-mixed flow-through or batch experiment. The fluid flow rate in the field is also much slower than in typical laboratory experiments. As a result, weathering in the field tends to be incongruent and to take place under near-equilibrium conditions. By contrast, most laboratory experiments are designed to achieve far from equilibrium conditions and to avoid precipitation of secondary minerals (e.g., Casey et al., 1993).

Neglecting the precipitation of secondary minerals would lead to incorrect estimates of the degree of saturation. The degree of saturation in the experiment with the biotite/chlorite-rich fraction was controlled by the balance between the increase in element concentrations due to the dissolution of the biotite and the decrease in concentrations due to the nontronite precipitation. If the dissolution of the biotite was congruent, the concentrations of Fe, Si and Al would be higher, and the biotite dissolution would be slower as a result of the increase in the degree of saturation. This conclusion is in agreement with those of Murakami et al. (1998) that the near equilibrium dissolution rate of anorthite is enhanced by precipitation of secondary minerals. Likewise, the degree of saturation in the field is a result of the balance between the dissolution of the primary minerals and the precipitation of the secondary minerals. In the absence of such precipitation, the dissolution of the primary minerals would be even slower than observed.

The behavior of plagioclase in the present study has exemplified the importance of coatings in minerals on dissolution kinetics. The rate of plagioclase dissolution increased with time by more than an order of magnitude due to the removal of the iron coating. Thermodynamic calculations using the EQ3NR code (Wolery, 1992) indicate that solutions in the present study were under-saturated with respect to iron oxides, leading to dissolution of the iron coatings. As iron was also released from biotite in the bulk granite experiment, the dissolution of the iron oxide coatings was closer to equilibrium, and therefore slower in the bulk granite experiment than in those using mineral-rich fractions. Thus, the increase in plagioclase dissolution rates was slower in the bulk granite experiment. In the field solutions may be oversaturated with Fe, as was observed by Murakami et al. (2003), and dissolution of iron-coated minerals would be strongly inhibited. Under such conditions, the amount of coating on plagioclase surfaces may even increase with time, although Murakami et al. (2003) observed that iron oxides mainly precipitate on the edges of biotite crystals.

Hodson (2003) precipitated an amorphous iron rich-coating on anorthite, and showed that this precipitate did not inhibit or slow the dissolution of the anorthite. He concluded that porous coatings on minerals in nature do not inhibit the dissolution of the coated minerals. In contrast to the artificial iron precipitate of Hodson (2003), the natural iron coating of the feldspar in the present study seems to inhibit mineral dissolution. Interestingly, our observations agree with unpublished data of Hodson that a naturally coated sample dissolved at a slower rate than an uncoated sample (Hodson, 2003). The different behavior of natural and artificial coating is not surprising and as Hodson (2003) noted, coatings on grains are highly varied both compositionally and morphologically. Inhibition of mineral dissolution due to surface coatings has also been observed in other studies (Mogollon et al., 1996; Nugent et al., 1998; Ganor et al., 1999; Metz et al., 2005). Our suggestion that the differences between laboratory and field dissolution rates may be at least partly attributed to mineral coatings is in agreement with the study of Nugent et al. (1998). Additional dissolution experiments with "dirty" naturally coated mineral samples are required to quantify the effect of coatings on the dissolution of minerals in the field.

The effect of drying on dissolution rates of the major minerals is intriguing. Whereas the dissolution of biotite is significantly enhanced, the dissolution rate of plagioclase decreased after drying. Before drying, the solution contained ~200 μM Fe. Precipitation of this iron on plagioclase surfaces may explain the slow rate of plagioclase dissolution during the subsequent dissolution stage. Enhancement of biotite dissolution rates following drying may reflect Fe oxidation during the drying period, which may have caused exfoliation of the edges of the biotite sheets as has been observed in weathered biotite from soils (e.g., Turpault and Trotignon, 1994; Murakami et al., 2003). An alternative explanation for the increase in biotite dissolution rate may be differential expansion of the different minerals (or of the same mineral in different directions) during drying at 50°C, which may improve the flow between the biotite grains and the bulk solution. This may increase the

degree of undersaturation near grain edges, and therefore enhance the biotite dissolution rate. The observations of the present study are insufficient to elucidate all the consequences of drying. As daily and seasonal cycles of wetting and drying are frequent natural phenomenon, further studies of the effect of drying are essential for understanding mineral dissolution in the field, and for comparing them to results obtained in fully-wetted laboratory dissolution experiments.

6. SUMMARY AND CONCLUSIONS

Plagioclase and microcline dissolved stoichiometrically during the dissolution of the bulk granite and the mineral separates. The measured steady state dissolution rates of both the plagioclase and microcline were within error the same in all of these experiments. The dissolution of the plagioclase was initially inhibited by an iron oxide coating on grain surfaces. The plagioclase dissolution rate increased almost linearly with the inferred decrease of iron coating on its surface. Due to biotite dissolution, iron concentration in solution in the bulk granite experiment was significantly higher than that in the experiments using the plagioclase- and the alkali feldspar-rich fractions. As a result, removal of iron coatings from grains within the bulk granite was slower, and consequently the rate of increase in the plagioclase dissolution rate was also slower. We suggest that such coatings may strongly inhibit dissolution rates in the field, especially under conditions in which dissolution of iron-bearing minerals increases iron concentration and consequently decreases the solubility of the coating.

In contrast to the dissolution of plagioclase and the perthitic alkali feldspar, dissolution of the biotite/chlorite in the bulk granite was significantly different than that in the biotite/chlorite-rich fraction. Whereas the biotite/chlorite-rich fraction dissolved incongruently under near-equilibrium conditions, biotite and chlorite within the bulk granite sample dissolved congruently under far from equilibrium conditions. These differences result from variations in the degree of saturation of the solutions with respect to both the dissolving biotite/chlorite and to the nontronite, which probably was precipitating during the dissolution of the biotite and chlorite-rich fraction. The two experiments were different in the water/biotite ratio, which led to differences in solution composition and saturation state. In contrast to most laboratory experiments, water/rock ratios in most soils and regoliths are very low, and as a result mineral dissolution in the field is typically non-congruent, and occurs under near equilibrium conditions.

The present study has demonstrated significant differences between dissolution rates of plagioclase and biotite/chlorite in the bulk Elat Granite and the dissolution rates of the constituent minerals in mineral-rich fractions, which were separated from the same granite sample. In the case of biotite, differences between the bulk granite experiment and the mineral-rich fraction were a result of differences in the abundance of the dissolving mineral. In the case of plagioclase, the presence of biotite in the granite affected the solution composition, inhibiting the dissolution of the iron oxide coatings and slowing the plagioclase dissolution. Both the presence of coatings and the near equilibrium conditions significantly reduce mineral dissolution rates in the field in comparison to the dissolution rate of clean minerals under far from equilibrium laboratory conditions. This conclusion is in agreement with White and Brantley (2003), who pointed out that the slower dissolution rate in the field compared to laboratory experiments is a result of both extrinsic differences (e.g., differences in saturation state) and intrinsic differences (e.g., surface coating).

Following the drying of the bulk granite the dissolution of biotite was significantly enhanced, whereas the dissolution rate of plagioclase was decreased. The observations of the present study demonstrate that to fully bridge the gap between the field and the laboratory mineral dissolution rates, both the effects of mineral coatings on dissolution rates and the effect of wetting and drying cycles should be further studied. More experiments are also required to study the effect of saturation state on mineral dissolution under different experimental conditions. The results of laboratory experiments should eventually be integrated into a full rate law for the dissolution reaction describing the combined effect of all environmental parameters.

Acknowledgments—This research was supported by Grant No. 1999-076-01 from the United States-Israel Binational Science Foundation (BSF), Jerusalem, Israel. We wish to express our gratitude to A. Zanvilevich, B. Litvinovsky, M. Eyal, H. Kisch and C. Zhu for fruitful and inspiring discussions. We thank the associate editor, Eric H. Oelkers, and three anonymous reviewers for their review of the manuscript. The manuscript was partly written during a sabbatical leave of the first author at the Department of Geology and Planetary Science, University of Pittsburgh, which is acknowledged for its warm hospitality.

Associate editor: E. H. Oelkers

REFERENCES

Acker J. G. and Bricker O. P. (1992) The influence of pH on biotite dissolution and alteration kinetics at low temperature. *Geochim. Cosmochim. Acta* **56** (*8*), 3073–3092.

Afifi A. A., Bricker O. P., and Chemerys C. J. (1985) Experimental chemical weathering of various bedrock types at different pH-values; 1. Sandstone and granite. *Chem. Geol.* **49** (1–3), 87–113.

Anbeek C. (1993) The effect of natural weathering on dissolution rates. *Geochim. Cosmochim. Acta* **57,** 4963–4975.

Barrante J. R. (1974) *Applied Mathematics for Physical Chemistry.* Prentice-Hall.

Blum A. and Stillings L. L. (1995) Feldspar dissolution kinetics. In *Chemical Weathering Rates of Silicate Minerals*, Vol. 31 (ed. A. F. White and S. L. Brantley), pp. 291–351. Mineralogical Society of America.

Brandt F., Bosbach D., Krawczyk-Barsch E., Arnold T., and Bernhard G. (2003) Chlorite dissolution in the acid pH-range: A combined microscopic and macroscopic approach. *Geochim. Cosmochim. Acta* **67** (*8*), 1451–1461.

Brunauer S., Emmett P. H., and Teller E. (1938) Adsorption of gases in multimolecular layers. *J. Am. Chem. Soc.* **60,** 309–319.

Casey W. H., Banfield J. F., Westrich H. R., and McLaughlin L. (1993) What do dissolution experiments tell us about natural weathering? *Chem. Geol.* **105,** 1–15.

Chou L. and Wollast R. (1984) Study of the weathering of albite at room temperature and pressure with a fluidized bed reactor. *Geochim. Cosmochim. Acta* **48,** 2205–2217.

Drever J. I. (2003) Surface and ground water, weathering and soils. In *Treatise on Geochemistry*, Vol. 5 (eds. H. D. Holland and K. K. Turekian). Elsevier Science, pp. 626.

Erel Y., Blum J. D., Roueff E., and Ganor J. (2004) Lead and strontium isotopes as monitors of experimental granitoid mineral dissolution. *Geochim. Cosmochim. Acta,* **68** (22), 4649–4663.

Eyal M., Litvinovsky B., Katzir Y., and Zanvilevich A. N. (in press) Pan-African high-potassium, calc-alkaline, peraluminous granites

from southern Israel: geology, geochemistry, and petrogenesis. *Journal of African Earth Sciences*.

Gaines R. V., Skinner H. C. W., Foord E. E., Mason B., and Rosenzweig A. (1997) *Dana's New Mineralogy: The System of Mineralogy of James Dwight Dana and Edward Salisbury Dana.* Wiley.

Ganor J., Mogollon J. L., and Lasaga A. C. (1999) Kinetics of gibbsite dissolution under low ionic strength conditions. *Geochim. Cosmochim. Acta* **63** (11–12), 1635–1651.

Gautier J. M., Oelkers E. H., and Schott J. (2001) Are quartz dissolution rates proportional to BET surface areas? *Geochim. Cosmochim. Acta* **65,** 1059–1070.

Helgeson H. C., Murphy W. M., and Aagaard P. (1984) Thermodynamic and kinetic constraints on reaction rates among minerals and aqueous solutions. II. Rate constants, effective surface area and the hydrolysis of feldspar. *Geochim. Cosmochim. Acta* **48,** 2405–2432.

Hodson M. E. (2003) The influence of Fe-rich coatings on the dissolution of anorthite at pH 2.6. *Geochim. Cosmochim. Acta* **67** (*18*), 3355–3363.

Malmstrom M. and Banwart S. (1997) Biotite dissolution at 25°C: The pH dependence of dissolution rate and stoichiometry. *Geochim. Cosmochim. Acta* **61** (*14*), 2779–2799.

Metz V., Amram K., and Ganor J. (2005) Stoichiometry of smectite dissolution reaction. *Geochim. Cosmochim. Acta,* in press.

Mogollon J. L., Ganor J., Soler J. M., and Lasaga A. C. (1996) Column experiments and the full dissolution rate law of gibbsite. *Am. J. Sci.* **296,** 729–765.

Murakami T., Kogure T., Kadohara H., and Ohnuki T. (1998) Formation of secondary minerals and its effect on anorthite dissolution. *Am. Mineral.* **83,** 1209–1220.

Murakami T., Utsunomiya S., Yokoyama T., and Kasama T. (2003) Biotite dissolution processes and mechanisms in the laboratory and in nature: Early stage weathering environment and vermiculitization. *Am. Mineral.* **88,** 377–386.

Nugent M. A., Brantley S. L., Pantano C. G., and Maurice P. A. (1998) The influence of natural mineral coatings on feldspar weathering. *Nature* **395,** 588–591.

Schnoor J. L. (1990) Kinetics of chemical weathering: A comparison of laboratory and field weathering rates. In *Aquatic Chemical Kinetics: Reaction Rates of Processes in Natural Waters* (ed. W. Stumm), pp. 475–504. Wiley.

Schweda P. S. (1989) Kinetics of alkali feldspar dissolution at low temperature. In *6th International Symposium on Water-Rock Interaction* (ed. Miles D. L.), Balkema, pp. 609–612.

Stumm W. (1992) *Chemistry of the Solid-Water Interface: Processes at the Mineral-Water and Particle-Water Interface in Natural Systems.* Wiley.

Taylor A., Blum J. D., Lasaga A., and MacInnis I. N. (2000) Kinetics of dissolution and Sr release during biotite and phlogopite weathering. *Geochim. Cosmochim. Acta* **64,** 1191–1208.

Turpault M.-P. and Trotignon L. (1994) The dissolution of biotite single crystals in dilute HNO_3 at 24°C: Evidence of an anisotropic corrosion process of micas in acidic solutions. *Geochim. Cosmochim. Acta* **58,** 2761–2775.

van Grinsven H. J. M. and van Riemsdijk W. H. (1992) Evaluation of batch and column techniques to measure weathering rates in soils. *Geoderma* **52** (1–2), 41–57.

Velbel M. A. (1993) Constancy of silicate-mineral weathering-rate ratios between natural and experimental weathering: Implications for hydrologic control of differences in absolute rates. *Chem. Geol.* **105,** 89–99.

White A. F. and Brantley S. L. (1995) Chemical weathering rates of silicate minerals. In *Reviews in Mineralogy*, Vol. 31 (ed. P. H. Ribbe), pp. 583. Mineralogical Society of America.

White A. F., Bullen T. D., Vivit D. V., and Schulz M. S. (1999) The role of disseminated calcite in the chemical weathering of granitoid rocks. *Geochim. Cosmochim. Acta* **63,** 1939–1953.

White A. F. and Brantley S. L. (2003) The effect of time on the weathering of silicate minerals: Why do weathering rates differ in the laboratory and field? *Chem. Geol.* **202,** 479–506.

Wolery T. J. (1992) *EQ3NR, a Computer Program for Geochemical Aqueous Speciation-Solubility Calculations: Theoretical Manual, User's Guide and Related Documentation (Version 7.0),* p. 262. Lawrence Livermore National Laboratory.